9082 *Macromolecules* **2009**, *42*, 9082–9088
DOI: 10.1021/ma901730a

Macromolecules
ARTICLE

Cylindrically Confined Diblock Copolymers

Priyanka Dobriyal,[†] Hongqi Xiang,[‡] Matsunaga Kazuyuki,[§] Jiun-Tai Chen,[†] Hiroshi Jinnai,[§] and Thomas P. Russell*,[†]

[†]*Department of Polymer Science and Engineering, University of Massachusetts, Amherst, Massachusetts 01003,* [‡]*Cabot Microelectronics, and* [§]*Kyoto Institute of Science and Technology, Kyoto, Japan*

Received August 3, 2009; Revised Manuscript Received September 11, 2009

ABSTRACT: Lamella-, cylinder-, and sphere-forming block copolymers (BCPs) of polystyrene-*b*-polybutadiene (PS-*b*-PBD) were drawn into the pores of anodized aluminum oxide (AAO) membranes in the melt by capillary forces. After thermal annealing, the nanorods of the BCP were removed by dissolution of the AAO with a weak acid, and transmission electron microscopy (TEM) was used to investigate the resultant morphologies of the confined BCPs. The diameters of the pores in the AAO and the molecular weight of the block copolymers were varied to investigate the effect of confinement on the microphase separation of the BCP. Concentric cylinders were observed for the lamella-forming BCPs under 2D confinement, and deviations of the lamella repeat period were measured as a function of AAO pore diameter. In addition, torus-like morphologies were observed as the degree of confinement increased. For the bulk cylinder-forming BCPs, a rich variety of morphologies, not seen in the bulk, were observed that included stacked torus-like morphologies and single-, double-, and triple-helical morphologies The specific morphology depended on D/L_0, where D is the AAO pore diameter and L_0 is the period of the BCP in the bulk. D/L_0 was varied from 0.92 to 2.22. For bulk sphere-forming BCPs, core−shell cylindrical morphologies, single columns of spherical microdomains, and spirals of doubly and triply paired spherical microdomains were observed. Transmission electron microscopy was also performed in tomography mode (TEMT) to quantitatively determine a 3-D description of the morphologies. The morphologies found were consistent with recent simulations of confined BCPs.

Introduction

Block copolymers (BCPs) have been the focus of a substantial body of experimental and theoretical investigation due to their ability to self-assemble periodic arrays of nanoscopic elements. BCPs are composed of two chemically distinct macromolecules covalently joined at one end. BCPs microphase separate into spherical, cylindrical, lamellar, and gyroid morphologies, depending on the volume fraction of the blocks where the size of the microdomains is dictated by the molecular weight of the BCP. These self-assembled structures serve as ideal templates and scaffolds that are finding use for the generation of low dielectric constant materials, sectored floating gates in flash memory, ultrahigh density magnetic storage media, and photovoltaic devices.[1−4] Controlling the response of BCPs to their environment so as to engineer novel nanoscopic structures is an emerging area of research that holds promise for further expanding the fabrication of nanoscopic structures. 3D confinement represents, perhaps, the simplest means of exerting an external field on a BCP where the dimensions of the confining volume are, at least in one, if not two directions, comparable to the repeat period of the BCP morphology in the bulk. One encounters such confinement in nanoimprinting where the dimensions of the features on the master are approaching the dimensions of a single polymer chain.[5]

The confinement of BCPs by two parallel solid walls represents the case of 1D confinement and has been studied in the past.[6−11] If the separation distance between the confining walls is not commensurate with the period of the BCP and there are strong preferential interactions of the blocks with the walls, then the repeat period of the BCP will change to compensate for the incommensurability. Consequently, the BCP chains will either stretch or compress to compensate. If, however, the interactions of the blocks with the walls are not strong or if the interactions are balanced, then the orientation of the microdomains will change from being parallel to being perpendicular to the confining walls.[12] A further degree of confinement can be produced by placing the BCP within the nanoscopic pores in an AAO membrane. Along the pores the BCP is unconstrained, while the walls of the pores radially confine the BCP. Parameters controlling the morphology of the confined BCP include the strength of the interactions of the blocks with the walls, commensurability between the pore diameter, D, and the natural period of the BCP morphology in the bulk, L_0, i.e., the structural frustration parameter, D/L_0, which gives rise to a stretching or compression of the BCP chains, and the curvature that is being forced on the BCP morphology due to the confinement within a pore where $D \sim L_0$, which forces a nonideal packing of the BCP chains at the interface between the microdomains. Previous studies on neat BCPs and BCPs with co solvents have shown that marked deviations of the morphology from the bulk can be obtained due to a combination of these factors. In addition, numerous theoretical studies have appeared wherein a wide variety of different morphologies are predicted by varying the above-mentioned parameters. 3D confinement of BCPs is far less explored; however, by use of aerosols or precipitation of colloidal BCP particles, such confinement can be achieved. Recently, both experimental and theoretical studies have appeared that touch on the myriad of morphologies that such confinement can produce.[13−16]

The 2D confinement of symmetric BCPs have been studied experimentally by Xiang et al. and Sun et al. where symmetric polystyrene-*b*-polybutadiene (PS-*b*-PBD) and polystyrene-*b*-poly(methyl methacrylate) (PS-*b*-PMMA) were confined within AAO membranes and concentric rings of lamella were observed.[17,18] Ma et al. also observed concentric lamella in their studies done on

*Corresponding author: Tel 1-413-545-2680; Fax 1-413-577-1510; E-mail russell@mail.pse.umass.edu.

 Published on Web 09/23/2009

Table 1. Characteristics of PS-*b*-PBD Block Copolymers

molecular weight (g/mol)	bulk morphology	center−center spacing (nm)	volume fraction (PS)
40 000	cylinder	32	0.71
46 000	cylinder	33	0.69
60 000	cylinder	41	0.72
74 000	sphere	32	0.84
18 000	lamella	20	0.51
28 000	lamella	28	0.49
30 000	lamella	29	0.51
42 000	lamella	40	0.51
78 000	lamella	65	0.52

polystyrene-*block*-polyisoprene nanowires.[19] He et al. performed Monte Carlo simulations, and Sevink et al. used dynamic density functional theory and predicted the concentric cylinders type of structure that can form when a symmetric diblock copolymer is cylindrically confined.[20,21] The influence of cylindrical confinement on the lamella thickness of symmetric BCP was addressed by Wang[22] in his Monte Carlo simulations and Yu et al.[23] in his simulated annealing technique. Xiang et al.[24] was able to observe the torus-like morphology for symmetric PS-*b*-PBD inside AAO when pore diameter was comparable to L_0 and D/L_0 was not an integer.

With asymmetric diblock copolymers, the morphologies of the confined BCPs deviate significantly from the bulk. Both confinement and the forced curvature break the symmetry of the bulk morphology, forcing the BCP to assume morphologies not seen in the bulk. This symmetry breaking is strongly dependent on the diameter of the pore confining the BCP, and hence, a large range of different morphologies emerge as a function of pore diameter. This, of course, can be used to advantage so as to engineer unique nanostructured morphologies that may open new opportunities for the fabrication of nanoscopic devices. Numerous groups have reported the simulation results on cylindrically confined BCPs that have a cylindrical microdomain morphology in the bulk.[25−28] Shi et al. focused on the interactions of BCPs with the pore wall: (a) when the pore wall attracts the majority block, (b) when the pore wall attracts the minority block, and (c) when pore wall is neutral toward both blocks.[29,30] A plethora of morphologies were predicted. Using self-consistent mean field theory, Li et al. developed a morphology diagram for BCPs under cylindrical confinement.[31,32] Experimentally, various morphologies were found to exist as a result of confining silica−surfactant composite inside the nanochannels of AAO.[33] In the case of copolymers, asymmetric BCPs of PS-*b*-PBD have been studied by Xiang et al. where a range of different morphologies were observed depending on D/L_0.[34,35] However, the number of different cases investigated was limited. Simulations have also been conducted for the bulk sphere-forming system under confinement, and morphologies like zigzags, helices, and others have been reported.[36,37] Experimentally, Thomas et al. have studied the self-assembly of spherical micelles in 2D confinement and observed the structures predicted in simulations.[38] Shi et al. carried out the calculations to investigate the effect of confinement on the body-centered-cubic phase of a BCP.[39,40]

In order to explore all the existing morphologies as a result of 2D confinement and to map their phase boundaries, pore diameter (D) and molecular weight of the copolymer need to be sequentially varied. In this paper, transitions in the morphologies of symmetric and asymmetric PS-*b*-PBD cylindrically confined within nanopores in AAO membranes were investigated using TEM as a function of the pore diameter. For this BCP, PBD preferentially segregates to the pore wall when the morphologies are longitudinally invariant along the pore axis. A quantitative treatment of the morphologies is presented with the use of AAO membranes prepared in house where the pore diameter can be finely controlled and where the pore diameter is uniform along the pores. In addition, TEMT was used to develop a 3D image of the morphologies where strong deviations from the bulk behavior of the BCP were found.

Experimental Section

Alumina membranes were prepared using a published two-step anodization process.[41−43] The electrolyte used was 0.3 M oxalic acid that was maintained at 17 °C. 40 V was applied to anodize polished Al sheets to produce 40−45 nm diameter pores with a length of ~80 μm in aluminum oxide. The AAO membranes were treated with 5 wt % aqueous H_3PO_4 solution at 30 °C to generate pores with diameters ranging from 40 to 80 nm.

The preparation of carbon-coated alumina membranes was described previously in detail.[44] In brief, a solution of polyacrylonitrile (PAN) in dimethylformamide (DMF) was introduced into the AAO membranes. After solvent evaporation, a thin film of PAN was left on the walls of the pores. After stabilization at 250 °C and the subsequent pyrolysis at 600 °C, PAN was converted to amorphous carbon, forming amorphous carbon-coated alumina membranes. Dissolution of the AAO membrane with a 5 wt % sodium hydroxide solution left free-standing amorphous carbon nanotubes (aCNTs). Prior to removal of the AAO membranes, the aCNTs were filled with BCPs using capillary force to draw the BCP into the aCNT. The aCNT served as an ideal support to maintain confinement of the BCP during subsequent electron microscopy studies.

All the symmetric and asymmetric PS-*b*-PBDs diblock copolymers were purchased from Polymer Source Inc. Details are given in Table 1 for symmetric and asymmetric BCP. Small-angle X-ray scattering (SAXS) experiments confirmed the bulk morphology of the BCP. To calculate volume fraction accurately, NMR was performed which yielded the PS volume fraction. A schematic diagram of the sample preparation is shown in Figure 1. A 10% solution of PS-*b*-PBD copolymer was prepared in toluene and drop-cast onto a clean glass slide. The resultant film was dried under vacuum for 24 h. Alumina membranes were placed on the top of the dried copolymer films and annealed under vacuum at 125 °C for 4 days. Capillary force drew the BCP into the membranes. The membranes were then removed in a 5 wt % sodium hydroxide (NaOH) to produce free-standing BCP nanorods. Samples for TEM were prepared by staining the BCP nanorods with an aqueous solution of osmium tetraoxide (OsO_4). These nanorods were then embedded in an epoxy resin which was purchased from Polysciences and consisted of three components: Araldite resin, dodecenylsuccnic anhydride, and DMP-30. The nanorods were placed on the resin, and then the resin was cured at 60 °C for 24 h. This temperature is sufficiently below the glass transition temperature of the PS in the BCP so that the morphology obtained with the BCP in the AAO membranes would be retained. The samples were cut into thin sections by using a Leica Ultracut microtome equipped with a diamond knife. TEM studies were performed using a JEOL 100CX operated at an accelerating voltage of 100 kV.

Results and Discussion

Typical TEM micrographs of nanorods of symmetric PS-*b*-PBD after removal from the AAO membrane are shown in

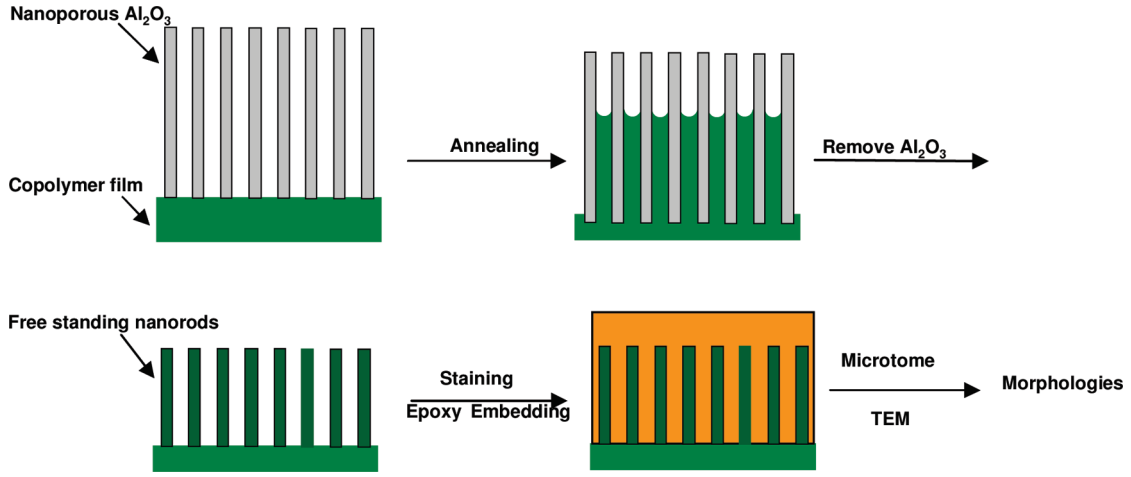

Figure 1. Schematic of sample preparation.

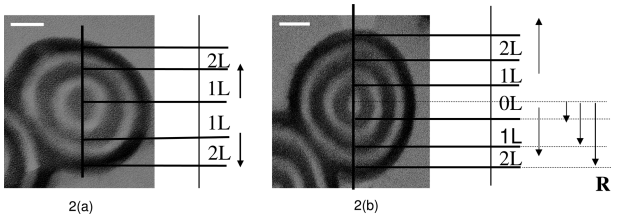

Figure 2. Morphology of bulk lamella forming diblock copolymers inside AAO nanopores and illustration of how the lamella period was measured. *R* is the distance from the center of the pore. Scale bar is 50 nm. (a) Odd number of bilayers (Ps and PBD) with a PBD core. (b) Even number of bilayers (PS and PBD) with PS core.

Figure 2. Since the nanorods were stained with osmium tertoxide (OsO_4), the PBD is dark in the images. As can be seen, concentric rings of PS and PBD form within the nanopore geometry. In all cases, PBD was found to preferentially segregate to the pore walls. Depending on the pore diameter, either PS or PBD formed a central core. The center-to-center distance (L) between consecutive PBD layers was measured. In cases where PDB formed the central core of the nanorod, the first period was taken from the center of the nanopores, i.e., the cylindrical microdomain running down the center of the nanorods, to the center of the first full band of PBD. This was termed $n1L$. Subsequent center-to-center distances between PBDs were termed $n2L$, $n3L$. In cases where PS formed the central core of the nanorod, the first period was taken as twice the distance from the center of the nanorod to the center of the first PBD band and was termed $n0L$. Subsequent periods were taken as the center-to-center distance between adjacent PBD layers and were termed nXL (where $X = 1, 2, 3, 4$, etc.). This is illustrated in Figure 2a,b. Depending on the diameter of the nanopore confining the PS-*b*-PBD and the number of concentric bands formed, the conditions of commensurability or frustration will change, and the period, as in the case of BCPs under planar confinement, may not be equal to L_0, the equilibrium period of the bulk BCP. In addition, the period of the BCP may not be constant as a function of the distance from the center of the nanorod. This, of course, reflects the influence of forced curvature on the packing of the BCP chains at the interfaces of the microdomains.

Shown in Figure 3a is the measured period of the PS-*b*-PBD, normalized by L_0, as a function of R, the distance from the center of the nanorod, normalized by L_0. Here, there are an even number of bands, and the core is PS and R was taken as the distance from the center of the nanorod to the center of the nth PBD ring. When the number of layers is odd, i.e., with a PBD core, a similar plot was constructed in Figure 3b with the normalized center-to-center distance between layers shown as a function of the reduced radial distance R/L_0. In general, in both parts a and b of Figure 3, the slopes of these data decrease with increasing distance from the center. These results suggest that the effect of curvature is most pronounced for the innermost layers or microdomains. For the case of an odd number of layers, the slopes of different lamellar period were plotted as a function of the layer number of the microdomain or layer in Figure 3c. As seen, the slope decreases as one proceeds from the center, as would be expected, since the influence of forced curvature decreases. In addition, like the results for lamellar block copolymers confined between parallel surfaces, a sawtooth plot emerges as the number of layers increase. This results from a balance between the stretching of the copolymer chains at the interfaces of the microdomains while maintaining a given number of layers, as opposed to adding an additional layer and compressing the copolymer chains. These results suggest that it is easier to stretch, as opposed to compress, the copolymer chains, as evidenced by the values of L/L_0 where the transition in adding an additional layer occurs. However, unlike the case of lamellar microdomains confined between parallel surfaces, the additional contribution of curvature to the free energy enables the copolymers to use another mechanism to minimize the free energy. In particular, the block copolymer can undergo a morphological transition. With increasing confinement, i.e., decreasing the pore diameter, at $D/L_0 = 2.6$, torus-like structures were observed for PS-*b*-PBD that form a lamellar morphology in the bulk. Figure 4a shows the cross-sectional view of the torus-like morphology when the nanorods were microtomed along the pore axis, and Figure 4b shows the view of the same sample when microtomed across the pore axis. In Figure 4a layers of PS stacked on top of one another, fully encase in PBD is seen, whereas down the nanorods axis, a concentric cylindrical morphology is seen. Consequently, a torus-like morphology forms which, in essence, preserves as much of the original bulk lamellar type of morphology under the constraints imposed.

For bulk cylinder forming PS-*b*-PBD, novel morphologies appeared as the D/L_0 was varied. Previous results by Xiang et al. on a similar BCP had indicated that there was a wetting layer of PBD on AAO surface, but this was limited to the case when the bulk morphology was maintained even within the AAO membranes, as for example cylinders aligning along the pore axis. With the increasing degree of confinement, though, the frustration imposed by the confinement was sufficient to overcome this preferential segregation of PBD to the pore walls. Figure 5a shows a TEM image of the torus-like nanostructure formed

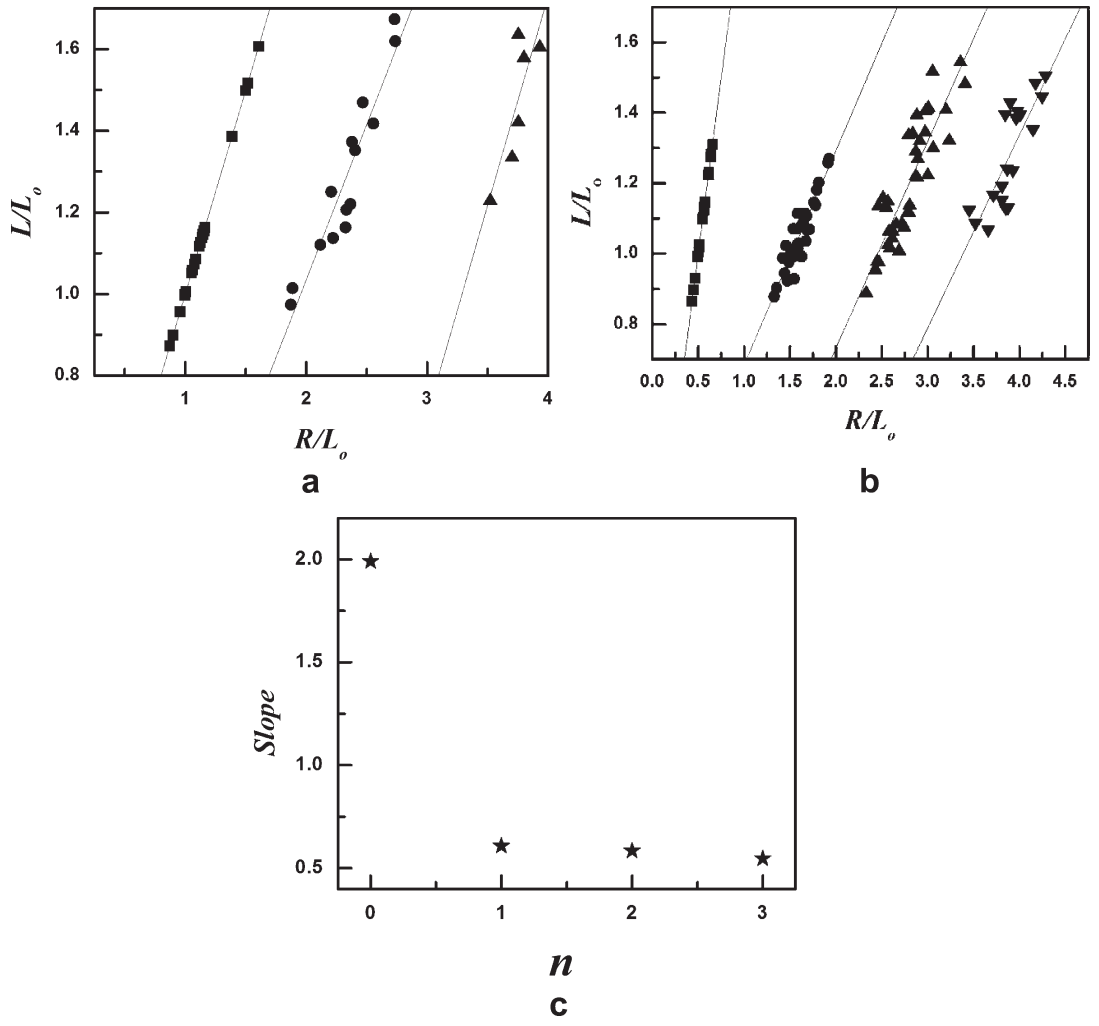

Figure 3. Center-to-center distance (L) between consecutive PBD layers plotted as a function of distance from the center of the pore. Both the period and the radius are normalized by the bulk equilibrium lamella period L_0. (a) $N = 4$: 6 (■) $n1L$, (●) $n2L$, (▲) $n3L$. (b) $N = 5, 7$: (■) $n0L$, (●) $n1L$, (▲) $n2L$, (▼) $n3L$. (c) Values of slopes for different bilayer (PS and PBD) thickness for $N = 5, 7$ plotted as a function of the number of layers from the center.

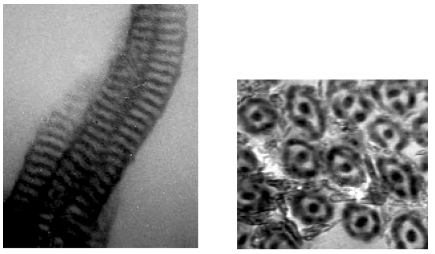

Figure 4. Torus-like morphology formed by bulk lamella-forming diblock copolymer inside AAO: (a) view along the pore axis; (b) view across the pore axis. Scale bar: 50 nm.

inside the AAO. Since PBD was stained with OsO_4, the darker regions in the TEM image arise from the PBD. Here, it is evident that PS, and not PBD, is located at the walls of the nanopores due to the volume fraction of PBD, the minor component, in the copolymer and the severe entropic penalty that would be required to locate PBD at the pore walls. TEM topographic (TEMT) images in Figure 5b−d show that the morphology of the PS-*b*-PBD actually consists of two different morphologies. One is a torus-like morphology while the second is a stack of PS disks. The origins of these two different morphologies arises from the variation in the diameter of the pore where for $D/L_0 = 0.92$ disks are observed and for $D/L_0 = 1$ a torus-like morphology is seen. With other AAO membranes, as D/L_0 increased from 1.2 to 1.57, single helices of PBD were found in a PS matrix, as shown in Figure 6a. In Figure 6b the TEMT image clearly shows the helical nature of this morphology. Upon further increasing D/L_0, double helices of PBD in a PS matrix were observed for D/L_0 ranging from 1.58 to 1.78. Parts a and b of Figure 7 show a TEM image and the TEMT for such a double-helix type of morphology, respectively. At $D/L_0 = 1.81$, rings of PBD with a PBD cylindrical core in the PS matrix were observed as shown in Figure 8a. When D/L_0 was changed from 1.84 to 2.1, single helices of PBD were found surrounding a PBD cylindrical core cylinder, as shown in Figure 8b and the corresponding TEMT images in Figure 8e,f. At $D/L_0 = 2.2$, double helices and triple helix of PBD with PBD cylindrical core cylinder were observed as shown in Figure 8c,d and in the corresponding TEMT images in Figure 8g, where a triple-helical morphology is shown. TEMT was found to be crucial in delineating these different morphologies formed during confinement. By increasing further, for $D/L_0 > 2.3$, single cylinders of PBD with PBD wetting layer on the wall are formed, as described previously by Xiang et al.[24] When this bulk cylinder-forming PS-*b*-PBD was introduced into an aCNT (amorphous carbon nanotube), where $D/L_0 = 1.96$, a single helix of PBD with a cylindrical PDB core was observed. The difference between the

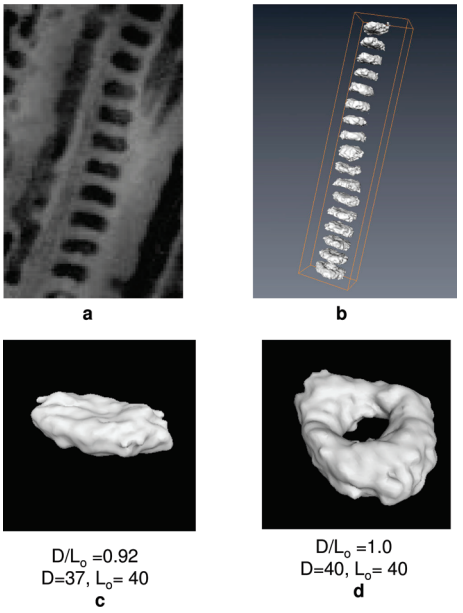

Figure 5. TEM image of the morphology formed by bulk cylinder-forming diblock copolymer inside AAO: (a) view across the pore axis; (b) TEMT image showing stacked disks and torus-like structures; (c) cross-sectional view of the stacked disks; (d) cross-sectional view of the torus-like structures. Scale bar: 50 nm.

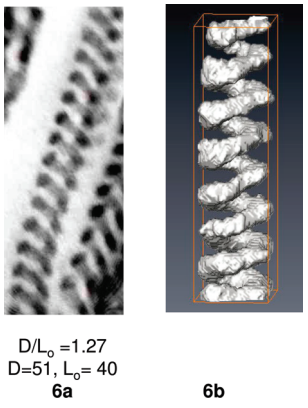

Figure 6. TEM images of bulk cylinder-forming BCP inside AAO. View along the AAO pore of a nanorod with (a) PBD single helix in PS matrix (b). Corresponding TEMT image. Scale bar: 50 nm.

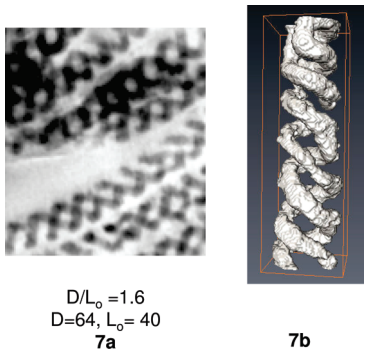

Figure 7. TEM images of bulk cylinder-forming BCP inside AAO. View along the AAO pore of a nanorod with (a) PBD double helix in PS matrix. (b) Corresponding TEMT image. Scale bar: 50 nm.

morphology within the aCNT and in the AAO membrane arises more than likely arises from the difference in the interfacial energies between the blocks and the walls of the nanopores.

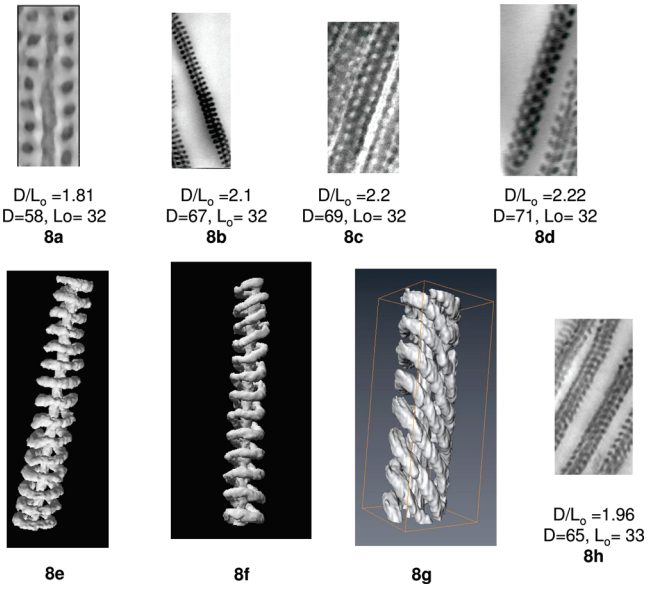

Figure 8. TEM images of bulk cylinder-forming BCP inside AAO. View along the AAO pore of a nanorod with (a) PBD core and ring in PS matrix, (b) PBD core and helix in PS matrix, (c) PBD core and double helix in PS matrix, (d) triple helix of PBD in PS matrix; (e) and (f) are the TEMT images corresponding to (a) and (b). (g) TEMT image of a PBD core and triple helix in PS matrix, and (h) view along an amorphous carbon nanotube (aCNT) with PBD core and helix in PS matrix. Scale bars: (a, h) 50 nm; (b−g) 100 nm.

While confinement was found to vary the morphology of the copolymer, the pitch of the helices (single, double, and triple) were found to depend upon the degree of confinement as well. The pitch, h, of the helical morphologies, normalized by the radius of the nanopores, r, as a function of D/L_0 for single, double, and triple helices of PBD in a PS matrix is shown in Figure 9. In all cases, as the diameters of the nanopores increase, the pitch of the PBD helices decreased. In no case were mixed structures observed except at the D/L_0 values where a transition between single and double helices occurred. We are not certain if this is related to the precision to which the diameter of the nanopores could be measured though. For $D/L_0 > 2.3$, a single cylinder of PBD formed running parallel to the axis of the nanopores. It was also observed that there was no presence for one specific handedness of the helical morphologies, with both right- and left-handed helices appearing in equal number for any value of D/L_0. This can be discerned in the micrograph shown in Figure 8b where both a right-handed and left-handed helix are seen to wrap around the central PBD core.

The range of morphologies observed in our studies was also observed in simulations by Wickham and co-workers using real space self-consistent mean field theory to study the self-assembly of an asymmetric BCP confined inside a cylindrical nanopore. Since the volume fraction of the BCP in their simulations does not precisely match with the volume fractions of the BCPs used in our studies, transitions in the morphologies were found at different values of D/L_0. However, the sequence in which the different morphologies appeared was in agreement with the simulations of Zhu et al.,[28,29] Yu et al.,[23,29,30] and Li et al.[31,32] One experimental difficulty that arose during our studies was the difficulty in quantitatively and consistently differentiating between the PS at the walls of the nanopores and the epoxy resin used to imbed the samples.

For bulk sphere forming PS-*b*-PBD copolymers, Figure 10 shows a series of TEM images containing different morphologies that were observed at different degrees of confinement D/L_0. For the highest degree of confinement, $D/L_0 = 1.1$, concentric

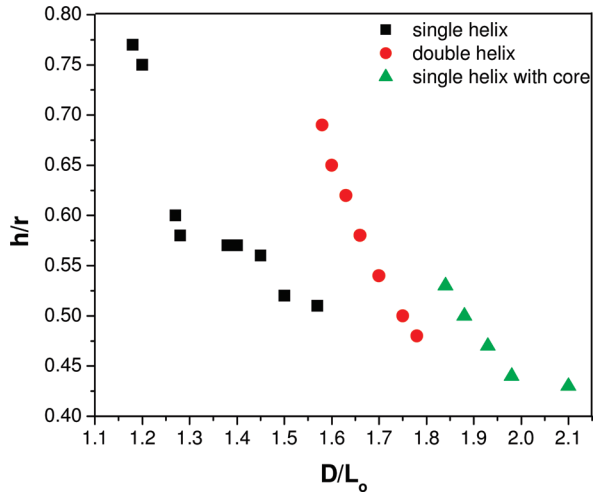

Figure 9. Pitch of helices normalized by pore radius h/r as a function of the noralized diameter D/L_0 for single and double helices and single helix with PBD core: (■) single helix, (●) double helix, and (▲) single helix with core.

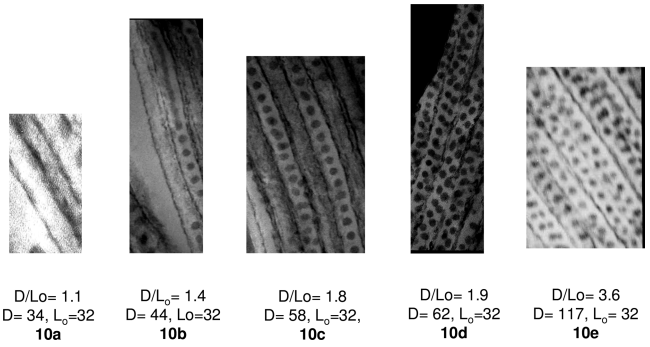

Figure 10. TEM images of bulk sphere forming BCP inside AAO. View along the AAO pore of a nanorod: (a) core shell cylinder; (b) one row of spheres; (c) two rows of spheres; (d) three rows of spheres. Scale bars: 50 nm.

cylinders were observed where PS formed the core and PBD formed a thin cylindrical shell around the PS core, as shown in Figure 10a. Unlike the PS-*b*-PBD having a cylindrical microdomain morphology in the bulk, even though PBD is the minor component, the formation of a brush of PBD at the interface between the PS and the nanopores wall occurred for these copolymers that formed spherical microdomains in the bulk. Upon increasing the pore diameter, for $D/L_0 = 1.4-1.8$, a different morphology was observed where a line of spherical PBD microdomains in a PS matrix formed along the central axis of the nanopores with a thin layer of PBD separating the PS from the walls of the nanopores, as shown in Figure 10b,c. By increasing pore diameter to 72 nm ($D/L_0 = 1.9$), the spherical microdomains were observed to form a zigzag pattern along the nanopores axis, as shown in Figure 10d. It is not known, at present, whether the microdomains are arranged along a helical path along the nanopores, since we were unsuccessful in our TEMT efforts. The transition from the zigzag type of pattern, where two spherical microdomains were observed, to a similar arrangement with three spherical was observed in 117 nm diameter pores ($D/L_0 = 3.65$), as shown in Figure 10d. For $d/L_0 > 3.65$, hexagonal arrangement of spheres was observed similar to the observation of Xiang et al.[17] In all cases, the center-to-center distance between the spherical microdomains was similar to that seen in the bulk. However, without the TEMT results, it is difficult to quantitatively assess this, since TEM offers only a 2-D projection of the morphology. It is clear, though, as the confinement of the microdomains increases, i.e., as the pore diameter decreases, the packing of the spherical microdomains changes in a systematic manner, and the PBD forms a thin layer between the PS matrix and the walls of the nanopores.

Conclusion

Morphologies and morphological transitions of PS-*b*-PBD block copolymers under 2-D confinement were studied. The molecular weights of the copolymers and the diameters of the nanopores in anodized aluminum oxide templates were varied to study the effect of confinement on the morphologies. It was found that under cylindrical confinement bulk lamellar-forming diblock copolymer forms concentric cylinders where the center-to-center distance between the layers forming the cylinders was found to vary with distance from the center of the confining nanopores. As the pore diameter became smaller, a transition in the morphology to torus-like structures was observed. For bulk cylinder-forming PS-*b*-PBD, the cylindrical nature of the minor component microdomains was preserved; however, the spatial arrangement deviated significantly from the hexagonally close-packed structure seen in the bulk. Torus-like morphologies and single-, double-, and triple-helical morphologies were observed, depending on the degree of confinement. With the helical morphologies, the pitches of the helices were found to depend on the degree of confinement, in general decreasing as the confinement decreased. For bulk sphere-forming PS-*b*-PBD, extreme confinement produced a core−shell type of morphology where, as the degree of confinement decrease, single rows of spherical microdomains and zigzag arrangements of the microdomains along the nanopores axes were observed. Transmission electron microscopy tomography was also used to generate 3-D images of the morphologies formed by the confined block copolymers and was essential in quantitatively defining the morphologies. With the ability to remove or chemically modify one of the microdomains, the morphologies induced by confinement offer a unique means of generating structures not observed in the bulk and a route to develop novel nanostructured materials.

Acknowledgment. This work was supported by the U.S. Department of Energy (DOE) and the NSF supported MRSEC at the University of Massachusetts Amherst.

References and Notes

(1) Park, C.; Yoon, J.; Thomas, E. L. Enabling nanotechnology with self assembled block copolymer patterns. *Polymer* **2003**, *44*, 6725–6760.
(2) Park, M.; Harrison, C.; Chaikin, P. M.; Register, R. A.; Adamson, D. H. Block copolymer lithography: periodic arrays of ~10^{11} holes in 1 square centimeter. *Science* **1997**, *276*, 1401–1404.
(3) Thurn-Albrecht, T.; Schotter, J.; Kastle, A.; Emley, N.; Shibauchi, T.; Elbaum, L.-K.; Guarini, K.; Black, C. T.; Tuominen, M. T.; Russell, T. P. Ultrahigh-density nanowire arrays grown in self-assembled diblock copolymer templates. *Science* **2000**, *290*, 2126–2129.
(4) Coakley, K. M.; McGehee, M. D. Photovoltaic cells made from conjugated polymers infiltrated into mesoporous titania. *Appl. Phys. Lett.* **2003**, *83*, 3380–3382.
(5) Chou, S. Y.; Krauss, P. R.; Renstrom, P. J. Imprint lithography with 25-nanometer resolution. *Science* **1996**, *272*, 85–87.
(6) Walton, D. G.; Kellogg, G. J.; Mayes, A. M.; Lambooy, P.; Russell, T. P. A free energy model for confined diblock copolymers. *Macromolecules* **1994**, *27*, 6225–6228.
(7) Shull, K. R. Mean-Field theory of block copolymers: Bulk melts, surfaces and thin films. *Macromolecules* **1992**, *25*, 2122–2133.
(8) Pickett, G. T.; Balazs, A. C. Equilibrium orientation of confined diblock copolymer films. *Macromolecules* **1997**, *30*, 3097–3103.
(9) Huang, E.; Russell, T. P.; Harrison, C.; Chaikin, P. M.; R. A.; Hawker, C. J.; Mays, J. Using surface active random copolymers to

control the domain orientation in diblock copolymer thin films. *Macromolecules* **1998**, *31*, 7641–7650.
(10) Koneripalli, N.; Singh, N.; Levicky, R.; Bates, F. S.; Gallagher, P. D.; Satija, S. K. Confined block copolymer thin films. *Macromolecules* **1995**, *28*, 2897–2904.
(11) Wang, Q.; Yan, Q.; Nealey, P. F.; de Pablo, J. J. Monte Carlo simulations of diblock copolymer thin films confined between two homogenous surfaces. *J. Chem. Phys.* **2000**, *112*, 450–464.
(12) Lambooy, P.; Russell, T. P.; Kellogg, G. J.; Mayes, A. M.; Gallagher, P. D.; Satija, S. K. Observed frustration in confined block copolymers. *Phys. Rev. Lett.* **1994**, *72*, 2899–2902.
(13) Arsenault, A. C.; Rider, D. A.; Tétreault, N.; Chen, J. I.; Coombs, N.; Ozin, G. A.; Manners, I. Block copolymers under periodic, strong three-dimensional confinement. *J. Am. Chem. Soc.* **2005**, *127*, 9954–9955.
(14) Yu, B.; Li, B.; Jin, Q.; Ding, D.; Shi, A.-C. Self-Assembly of symmetric diblock copolymers confined in spherical nanopores. *Macromolecules* **2007**, *40*, 9133–9142.
(15) Higuchi, T.; Tajima, A.; Motoyoshi, K.; Yabu, H.; Shimomura, M. Frustrated phases of block copolymers in nanoparticles. *Angew. Chem., Int. Ed.* **2008**, *47*, 8164–8166.
(16) Thomas, E. L.; Refner, J. R.; Bellare, J. A menagerie of interface structures in copolymer systems. *J. Phys. Colloq.* **1990**, *51*, C7-363−C7-374.
(17) Xiang, H.; Shin, K.; Kim, T.; Moon, S. I.; McCarthy, T. J.; Russell, T. P. Block copolymers under cylindrical confinement. *Macromolecules* **2004**, *37*, 5660–5664.
(18) Sun, Y.; Steinhart, M.; Zschech, D.; Adhikari, R.; Michler, G. H.; Gosele, U. Diameter-Dependence of the morphology of PS-*b*-PMMA Nanorods, Confined Within Ordered Porous Alumina templates. *Macromol. Rapid Commun.* **2005**, *26*, 369–375.
(19) Ma, M.; Krikorian, V.; Yu, J. H.; Thomas, E. L.; Rutledge, G. C. Electrospun Polymer Nanofibers with Internal Periodic Structure Obtained by Microphase Separation of Cylindrically Confined Block Copolymers. *Nano Lett.* **2006**, *6*, 2969–2972.
(20) He, X.; Song, M.; Liang, H.; Pan, C. Self-assembly of the symmetric diblock copolymer in a confined state: Monte Carlo simulation. *J. Chem. Phys.* **2001**, *114*, 10510.
(21) Sevink, G. J. A.; Zvelindovsky, A. V.; Fraaije, J. G. E. M. *J. Chem. Phys.* **2001**, *115*, 8226–8230.
(22) Wang, Q. Symmetric diblock copolymers in nanopores: Monte Carlo simulations and strong-stretching theory. *J. Chem. Phys.* **2007**, *126*, 024903–11.
(23) Yu, B.; Sun, P.; Chen, T.; Jin, Q.; Ding, D.; Li, B.; Shi, A.-C. Self-assembly of diblock copolymers confined in cylindrical nanopores. *J. Chem. Phys.* **2007**, *127*, 114906–15.
(24) Xiang, H.; Shin, K.; Moon, S. I.; Kim, T.; McCarthy, T. J.; Russell, T. P. Curving and frustrating flatlands. *Science* **2004**, *306*, 76.
(25) Xiao, X.; Huang, Y.; Liu, H.; Hu, Y. Morphology Transition of Block Copolymers under Curved Confinement. *Macromol. Theory Simul.* **2007**, *16*, 732–741.
(26) Maniadis, P.; Tsimpanogiannis, I. N.; Kober, E. M.; Lookman, T. Phase segregation of diblock copolymers in nanopore geometries. *Europhys. Lett.* **2008**, *81*, 56001–6.
(27) Sevink, G. J. A.; Zvelindovsky, A. V. Block copolymers confined in a nanopore: Pathfinding in a curving and frustrating flatland. *J. Chem. Phys.* **2008**, *128*, 084901–16.
(28) Zhu, Y.; Jiang, W. Self-assembly of diblock copolymer mixtures in confined states: A Monte Carlo study. *Macromolecules* **2007**, *40*, 2872–2881.
(29) Yu, B.; Jin, Q.; Ding, D.; Li, B.; Shi, A.-C. Confinement-induced morphologies of cylinder-forming asymmetric diblock copolymers. *Macromolecules* **2008**, *41*, 4042–4054.
(30) Yu, B.; Sun, P.; Chen, T.; Jin, Q.; Ding, D.; Li, B.; Shi, C.-A. Confinement-induced novel morphologies of block copolmyers. *Phys. Rev. Lett.* **2006**, *96*, 138306−1–138306−4.
(31) Li, W.; Wickham, R. A.; Garbary, R. A. Phase diagram of a diblock copolymer melt under cylindrical confinement. *Macromolecules* **2006**, *39*, 806–811.
(32) Li, W.; Wickham, R. A. Self-Assembled morphologies of a diblock copolymer melt confined in a cylindrical nanopore. *Macromolecules* **2006**, *39*, 8492–8498.
(33) Wu, Y.; Cheng, G.; Katsov, K.; Sides, S. W.; Wang, J.; Tang, J.; Fredrickson, G. H.; Moskovits, M.; Stucky, G. D. Composite mesostructures by nano-confinement. *Nat. Mater.* **2004**, *3*, 816–822.
(34) Xiang, H.; Shin, K.; Kim, T.; Moon, S. I.; McCarthy, T. J.; Russell, T. P. The influence of confinement and curvature on the morphology of block copolymers. *J. Polym. Sci., Part B: Polym. Phys.* **2005**, *43*, 3377–3383.
(35) Xiang, H.; Shin, K.; Kim, T.; Moon, S. I.; McCarthy, T. J.; Russell, T. P. From cylinders to helices upon confinement. *Macromolecules* **2005**, *38*, 1055–1056.
(36) Troch, K. S.; Coluci, V. R.; Braga, S. F.; Chinellato, D. D.; Sato, F.; Legoa, S. B.; Rurali, R.; Galva, D. G. Prediction of ordered phases of encapsulated C60, C70, and C78 inside carbon nanotubes. *Nano Lett.* **2005**, *5*, 349–355.
(37) Pickett, G. T.; Gross, M.; Okayama, H. Spontaneous chirality in simple systems. *Phys. Rev. Lett.* **2000**, *85*, 3652–3655.
(38) Thomas, A.; Schierhorn, M.; Wu, Y.; Stucky, G. Assembly of spherical micelles in 2D physical confinements and their replication into mesoporous silica nanorods. *J. Mater. Chem.* **2007**, *17*, 4558–4562.
(39) Tan, H.; Yan, D.; Shi, A.-C. Surface effect on the body centered-cubic phase of diblock copolymers. *Macromolecules* **2004**, *37*, 9646–9653.
(40) Tan, H.; Song, Q.; Yang, S.; Yan, D.; Shi, A.-C. Confinement effect on the Body-centered cubic phase of diblock copolymer in thin film, Macromolecular theory and Simulations. *Macromolecules* **2008**, *17*, 45–51.
(41) Masuda, H.; Yamada, H.; Satoh, M.; Asoh, H.; Nakao, M.; Tamamure, T. Highly ordered nano channel architecture in anodic alumina. *Appl. Phys. Lett.* **1997**, *71*, 2770–2772.
(42) Li, A. P.; Muller, F.; Birner, A.; Nielsch, K.; Gosele, U. Hexagonal pore arrays with a 50−420 nm interpore distance formed by self-organization in anodic alumina. *J. Appl. Phys.* **1998**, *84*, 6023–6026.
(43) Masuda, H.; Fukuda, K. Ordered Metal nanohole arrays made by a two step replication of honey comb structures of anodic alumina. *Science* **1995**, *268*, 1466–1468.
(44) Chen, J.-T.; Shin, K.; Leiston-Belanger, J. M.; Zhang, M.; Russell, T. P. Amorphous carbon nanotubes with tunable properties via template wetting. *Adv. Funct. Mater.* **2006**, *16*, 1476–1480.